

# CONTROLLER DESIGN AND PERFORMANCE STUDY OF DC-DC BIDIRECTIONAL CONVERTER FOR SPEED REGULATION OF PERMANENT MAGNET DIRECT CURRENT MACHINE

Pritam Kumar Gayen<sup>1</sup> – Sudip Das<sup>2\*</sup>

<sup>1</sup>Department of Electrical Engineering, Kalyani Government Engineering College, Kalyani, West Bengal, India

<sup>2</sup>Department of Electrical Engineering, JIS College of Engineering, Kalyani, West Bengal, India

---

## ARTICLE INFO

### Article history:

Received: 03.01.2024.

Received in revised form: 14.04.2024.

Accepted: 10.09.2024.

### Keywords:

PMDC machine

Speed controller design

Bidirectional DC-DC converter

Dynamic performance

Stability margin.

DOI: <https://doi.org/10.30765/er.2431>

---

## Abstract:

*This paper presents the design of a controller for a bidirectional DC-DC converter for speed control of a permanent magnet DC machine (PMDC). In recent years, this electric drive system has often been used in electric vehicles or hybrid electric vehicles. In this application, the development of a controller is required to support the various functions of the machine. The design methodology of the controller should provide satisfactory dynamic performance under both motor and generator operation of the PMDC machine. In this regard, the control of the bidirectional DC/DC converter is necessary. From the perspective of speed control, the condition for absolute stability is derived from the small-signal model of the PMDC drive system. Then the Ziegler-Nichols tuning table is used to determine the gain of the proportional-integral (PI) controller in the conventional way. From further investigation, it was found that the transient response and stability margin of the speed control loop in the conventional case are*

---

## 1 Introduction

In the modern age, electric or hybrid electric vehicles (EVs or HEVs) [1-3] are becoming increasingly important in order to reduce the consumption of petroleum fuel and the associated pollution. Research on technological aspects is also increasing for improved vehicle performance. In many parts of the world, the grid penetration level of distributed generation (DG) is increasing rapidly. In this context, EVs and HEVs are integrated with the local grid [4, 5] to improve the reliability and efficiency of the overall power network. The bidirectional power transfer between the grid and the vehicle [6, 7] is known as V2G or grid-to-vehicle (G2V) operations. A permanent magnet DC (PMDC) machine-based electric drive system [8–10] is extensively used in the vehicle. The battery discharges to provide the driving force for the wheel [11]. On the other hand, it must absorb regenerative energy from the machine when braking or travelling downhill [10]. In an EV or HEV application, the charging and discharging processes of the battery are normally carried out via the control of a bidirectional DC-DC converter [12-14]. In driving mode, the variable load torque on the drive wheel must be supported by the drive system. In this situation, proper execution of the speed control loop [15–17] is necessary. The speed controller adjusts the input voltage to the motor. Here, the duty cycle of the power converter is controlled to maintain the required amount of input voltage. Various non-linear and robust control techniques [18-23] are reported in different literatures for regulating a DC machine's speed. But the PI controller is widely adopted in practice due to its simplicity and ease of implementation. The design of the proportional-integral (PI) gains in the speed control loop is an important prerequisite as it determines the transient behaviour and the relative stability of the system. It can be mentioned here that the controller is extensively used in the industry. The PI gains are conventionally determined from the Ziegler-Nichols tuning

---

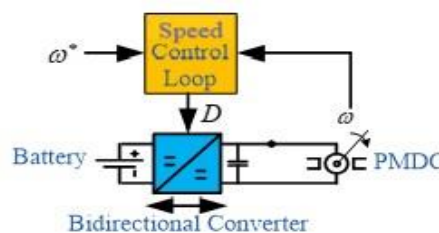
\* Corresponding author

E-mail address: [sudip.das@jiscollege.ac.in](mailto:sudip.das@jiscollege.ac.in)

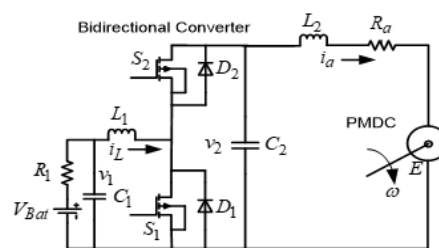
chart [10, 15, 24]. The traditional approach cannot always provide a good dynamic response under the various operational modes of a PMDC machine. Also, the stability margin is not high enough, and thus, there is a chance of failure during a system disturbance. Therefore, the work of this paper searches for superior controller gains so that improved transient performance as well as a stronger stability margin can be achieved under variable operations in both modes (motoring and regenerative). In this connection, various parameters of dynamic response and relative stability are exhaustively investigated using step response, root locus, and Bode plots under various operational modes, i.e., different loads and regeneration conditions as well as variable speed conditions. From wide investigation, common PI gains are decided for both operational modes of PMDC, which provide superior performance over conventional gains. The superior performance of the PMDC-based drive system in the proposed case is verified with the help of the MATLAB-SIMULINK software-based model. This paper also provides a large signal analysis of the proposed design's ability to maintain stability during significant and sudden changes in load torque. The information is critical for evaluating its performance in real-world settings. Including a large signal stability analysis is essential to gaining a complete understanding of the proposed speed controller's design. In this context, analytical evidence is provided. Various parts of the paper are formed as follows: The small- signal model of the PMDC drive system is presented in section 2. The determination of the absolute stability condition for the system in speed-controlled mode is described in Section 3 and the tuning process of the PI controller for the conventional control loop is also described in Section 3. Section 4 demonstrates the superior tuning process to achieve significantly improved dynamic response and relative stability through comparative evaluation. Large signal analysis is discussed in Section 5. Section 6 validates the improved performance in the proposed case through a MATLAB-SIMULINK software-based model. Section 7 presents experimental work and results. This paper is concluded in Section 8 and the conclusion section contains references.

## 2 Methodology of Small Signal State Space Model

The battery-fed PMDC drive with speed control loop is shown in Figure 1, which is focused on in the study of this paper. Here, the power converter supports bidirectional current under the motor and regenerative modes of operation of the machine, and it also controls the input voltage applied to the motor. The voltage is adjusted due to the action of the speed controller if the load torque or speed reference is changed, and finally, the desired speed is achieved. Thus, this paper concentrates on finding out the common gains of speed controllers, irrespective of the type of mode or loading conditions. At the same time, common performance criteria with sound transient performance (rise time, peak overshoot, and settling time) and a strong stability margin (gain and phase margin) will be maintained.



(a) Systematic diagram of overall system with speed control loop



(b) Circuit diagram

Figure 1. Battery-fed DC-DC bidirectional converter for supporting PMDC machine.

### 2.1 Large Signal Model

From Figure 1(b), the dynamic equations are formed in Eq. (1) under the condition - 'S<sub>1</sub>' is ON and 'S<sub>2</sub>' is OFF.

$$\begin{cases} \frac{di_L}{dt} = \frac{v_1}{L_1} \\ \frac{dv_1}{dt} = -\frac{v_1}{R_1 C_1} - \frac{i_L}{C_1} + \frac{V_{Bat}}{R_1 C_1} \\ \frac{di_a}{dt} = \frac{v_2}{L_2} - \frac{R_a i_a}{L_2} - \frac{k \cdot \omega}{L_2} \\ \frac{dv_2}{dt} = -\frac{i_a}{C_2} \\ \frac{d\omega}{dt} = \frac{k i_a}{J} - \frac{B \cdot \omega}{J} - \frac{T_L}{J} \end{cases} \quad (1)$$

From Eq. (1), state and output equations can be generally given in matrix form as,

$$\begin{cases} [\dot{X}] = [A_{ON}][X] + [B_{ON}][U] \\ [Y] = [C_{ON}][X] + [D_{ON}][U] \end{cases} \quad (2)$$

In (2), states, input and output variables are provided as,  $[X]^T = [i_L \quad v_1 \quad i_a \quad v_2 \quad \omega]$ ,  $[U]^T = [V_{Bat} \quad T_L]$ ,  $Y = \hat{\omega}$ , The ' $A_{ON} B_{ON} C_{ON} D_{ON}$ ' matrices of (2) is expressed as,

$$\begin{cases} [A_{ON}] = \begin{bmatrix} 0 & 1/L_1 & 0 & 0 & 0 \\ -1/C_1 & -1/R_1 C_1 & 0 & 0 & 0 \\ 0 & 0 & -R_a/L_2 & 1/L_2 & -k/L_2 \\ 0 & 0 & -1/C_2 & 0 & 0 \\ 0 & 0 & k/J & 0 & -B/J \end{bmatrix} \\ [B_{ON}] = \begin{bmatrix} 0 & 0 \\ 1/R_1 C_1 & 0 \\ 0 & 0 \\ 0 & 0 \\ 0 & -1/J \end{bmatrix} \\ [C_{ON}] = [0 \quad 0 \quad 0 \quad 0 \quad 1] \\ [D_{ON}] = [0 \quad 0] \end{cases} \quad (3)$$

Now, in other switching state i.e., ‘ $s_1$ ’ is OFF and ‘ $s_2$ ’ is ON, the governing equations are expressed as,

$$\begin{cases} \frac{di_L}{dt} = \frac{v_1}{L_1} - \frac{v_2}{L_1} \\ \frac{dv_1}{dt} = -\frac{v_1}{R_1 C_1} - \frac{i_L}{C_1} + \frac{V_{Bat}}{R_1 C_1} \\ \frac{di_a}{dt} = \frac{v_2}{L_2} - \frac{R_a i_a}{L_2} - \frac{k \cdot \omega}{L_2} \\ \frac{dv_2}{dt} = \frac{i_L}{C_2} - \frac{i_a}{C_2} \\ \frac{d\omega}{dt} = \frac{k i_a}{J} - \frac{B \cdot \omega}{J} - \frac{T_L}{J} \end{cases} \quad (4)$$

Eq. (4) can be generally written in matrix form as,

$$\begin{cases} [\dot{X}] = [A_{OFF}][X] + [B_{OFF}][U] \\ [Y] = [C_{OFF}][X] + [D_{OFF}][U] \end{cases} \quad (5)$$

In (5), elements of ‘ $A_{OFF} B_{OFF} C_{OFF} D_{OFF}$ ’ matrices are provided as,

$$\begin{cases} [A_{ON}] = \begin{bmatrix} 0 & 1/L_1 & 0 & 0 & 0 \\ -1/C_1 & -1/R_1 C_1 & 0 & 0 & 0 \\ 0 & 0 & -R_a/L_2 & 1/L_2 & -k/L_2 \\ 0 & 0 & -1/C_2 & 0 & 0 \\ 0 & 0 & k/J & 0 & -B/J \end{bmatrix} \\ [B_{ON}] = \begin{bmatrix} 0 & 0 \\ 1/R_1 C_1 & 0 \\ 0 & 0 \\ 0 & 0 \\ 0 & -1/J \end{bmatrix} \\ [C_{ON}] = [0 \ 0 \ 0 \ 0 \ 1] \\ [D_{ON}] = [0 \ 0] \end{cases} \quad (6)$$

## 2.2 Average State Space Model

The average values of matrices can be computed using (7) as,

$$\begin{cases} [A] = [A_{ON}] \cdot d + [A_{OFF}] \cdot (1-d) \\ [B] = [B_{ON}] \cdot d + [B_{OFF}] \cdot (1-d) \\ [C] = [C_{ON}] \cdot d + [C_{OFF}] \cdot (1-d) \\ [D] = [D_{ON}] \cdot d + [D_{OFF}] \cdot (1-d) \end{cases} \quad (7)$$

In (7), ‘ $d$ ’ represents duty cycle. The average value of state space and output matrices are given by,

$$\left\{ \begin{array}{l} [A] = \begin{bmatrix} 0 & 1/L_1 & 0 & -(1-d)/L_1 & 0 \\ -1/C_1 & -1/R_1C_1 & 0 & 0 & 0 \\ 0 & 0 & -R_a/L_2 & 1/L_2 & -k/L_2 \\ (1-d)/C_2 & 0 & -1/C_2 & 0 & 0 \\ 0 & 0 & k/J & 0 & -B/J \end{bmatrix} \\ [B] = \begin{bmatrix} 0 & 0 \\ 1/R_1C_1 & 0 \\ 0 & 0 \\ 0 & 0 \\ 0 & -1/J \end{bmatrix} \\ [C] = [0 \ 0 \ 0 \ 0 \ 1] \\ [D] = [0 \ 0] \end{array} \right. \quad (8)$$

### 2.3 Small Signal Model

The state space and output equations in terms of steady state and small signal variations part can be written as,

$$\left\{ \begin{array}{l} \begin{bmatrix} p(I_L + \hat{i}_L) \\ p(V_1 + \hat{v}_1) \\ p(I_a + \hat{i}_a) \\ p(V_2 + \hat{v}_2) \\ p(\omega + \hat{\omega}) \end{bmatrix} = \begin{bmatrix} 0 & 1/L_1 & 0 & -(1-D-\hat{d})/L_1 & 0 \\ -1/C_1 & -1/R_1C_1 & 0 & 0 & 0 \\ 0 & 0 & -R_a/L_2 & 1/L_2 & -k/L_2 \\ (1-D-\hat{d})/C_2 & 0 & -1/C_2 & 0 & 0 \\ 0 & 0 & k/J & 0 & -B/J \end{bmatrix} \begin{bmatrix} I_L + \hat{i}_L \\ V_1 + \hat{v}_1 \\ I_a + \hat{i}_a \\ V_2 + \hat{v}_2 \\ \omega + \hat{\omega} \end{bmatrix} \\ + \begin{bmatrix} 0 & 0 \\ 1/R_1C_1 & 0 \\ 0 & 0 \\ 0 & 0 \\ 0 & -1/J \end{bmatrix} \begin{bmatrix} V_{Bat} + \hat{V}_{Bat} \\ T_L + \hat{T}_L \end{bmatrix} \\ [p(Y + \hat{y})] = [0 \ 0 \ 0 \ 0 \ 1] \begin{bmatrix} (I_L + \hat{i}_L) \\ (V_1 + \hat{v}_1) \\ (I_a + \hat{i}_a) \\ (V_2 + \hat{v}_2) \\ (\omega + \hat{\omega}) \end{bmatrix} \end{array} \right. \quad (9)$$

In (9), derivative operator is symbolized as ‘ $p$ ’. Finally, small signal model is derived in terms of small variation of control input ( $\hat{d}$ ) as,

$$\begin{cases} \begin{bmatrix} p(\hat{i}_L) \\ p(\hat{v}_1) \\ p(\hat{i}_a) \\ p(\hat{v}_2) \\ p(\hat{\omega}) \end{bmatrix} = \begin{bmatrix} 0 & 1/L_1 & 0 & -(1-D)/L_1 & 0 \\ -1/C_1 & -1/R_1C_1 & 0 & 0 & 0 \\ 0 & 0 & -R_a/L_2 & 1/L_2 & -k/L_2 \\ (1-D)/C_2 & 0 & -1/C_2 & 0 & 0 \\ 0 & 0 & k/J & 0 & -B/J \end{bmatrix} \begin{bmatrix} \hat{i}_L \\ \hat{v}_1 \\ \hat{i}_a \\ \hat{v}_2 \\ \hat{\omega} \end{bmatrix} + \begin{bmatrix} V_2/L_1 \\ 0 \\ 0 \\ -I_L/C_2 \\ 0 \end{bmatrix} [\hat{d}] \\ \\ [p(\hat{y})] = [0 \ 0 \ 0 \ 0 \ 1] \begin{bmatrix} \hat{i} \\ \hat{v}_1 \\ \hat{i}_a \\ \hat{v}_2 \\ \hat{\omega} \end{bmatrix} \end{cases} \quad (10)$$

Table 1. Values of various rated parameters of Figure 1(b).

Parameters	Values
PMDC Machine	5 HP, 240 V, 15.92 A, 196.68 rad/s
$V_{Bat}, V_2$	52.15 V, 240 V
$I_L$	71 A
$R_1, R_a$	0.016667 $\Omega$ , 2.581 $\Omega$
$L_1, L_2$	10 $\mu$ H, 28 mH
$C_1, C_2$	10 mF, 10 mF
$J, B$	0.02215 kg/m <sup>2</sup> , 0.002953 Nm-s
$k$	(16.1/15.92) Nm/A
$D$	0.7826

### 3 Determination of Absolute Stability Conditions and Gains of PI Controller Using Conventional Approach

The process is described in reference to specifications of physical system components given in Table 1. The matrices of small signal model in (10) are computed using parameter values of Table I and these are presented below,

$$\begin{cases} [A] = \begin{bmatrix} 0 & 10^5 & 0 & -21.74e+3 & 0 \\ -100 & -6e+3 & 0 & 0 & 0 \\ 0 & 0 & -92.18 & 35.7143 & -36.12 \\ 21.74 & 0 & -100 & 0 & 0 \\ 0 & 0 & 45.6572 & 0 & -0.1333 \end{bmatrix}; [B] = \begin{bmatrix} 24e+6 \\ 0 \\ 0 \\ -7.1e+3 \\ 0 \end{bmatrix} \\ [C] = [0 \ 0 \ 0 \ 0 \ 1]; [D] = [0] \end{cases} \quad (11)$$

Thus, small signal transfer function from the ratio output voltage to duty cycle can be calculated as,

$$G(s) = \frac{\hat{\omega}}{\hat{d}} = \frac{-1.158e007.s^2 + 7.813e011.s + 4.989e015}{s^5 + 6092.s^4 + 1.103e7.s^3 + 3.834e9.s^2 + 3.149e11.s + 4.716e12} \quad (12)$$

The characteristics equation can be formed as,

$$1 + \frac{K(-1.158e007.s^2 + 7.813e011.s + 4.989e015)}{s^5 + 6092.s^4 + 1.103e7.s^3 + 3.834e9.s^2 + 3.149e11.s + 4.716e12} = 0 \tag{13}$$

In (13), ‘K’ indicates gain. The Routh array can be formed from (13) as,

$S^5$	1	1.103e7	3.149e11 + 7.813e11.K	
$S^4$	6092	3.834e9 - 1.158e7.K	4.716e12 + 4.989e15.K	
$S^3$	$\frac{63.361e9 + 1.158e7.K}{6092}$	$\frac{1.9137e15 - 0.2293e15.K}{6092}$	0	
$S^2$	$\frac{231.268e18 + 70.758e16.K - 1.34e14.K^2}{63.361e9 + 1.158e7.K}$	4.716e12 + 4.989e15.K	0	(14)
$S^1$	$\frac{423.645e33 - 20.0817e36.K - 748.356e31.K^2 - 6.383e29.K^3}{6092(231.268e9 + 70.758e16.K - 1.34e14.K^2)}$	0	0	
$S^0$	4.716e12 + 4.989e15.K	0	0	

Then absolute stability condition is found from (14) using Routh-Hurwitz criterion as,

$$K \leq 0.02109 \tag{15}$$

Thus, the ultimate or critical value of gain ( $K_u$ ) is taken from (15) as,

$$K_u = 0.02109 \tag{16}$$

Corresponding critical frequency ( $\omega_{cr}$ ) and ultimate time period ( $T_u$ ) are calculated from Routh array in respect of ‘S<sup>2</sup>’ row as,

$$\begin{cases} \omega_{cr} = 173.569 \text{ rad / sec} \\ \Rightarrow T_u = 0.0362 \text{ sec} \end{cases} \tag{17}$$

Now, PI gains from Ziegler-Nichols tuning chart are given as,

$$\begin{cases} K_p = 0.45 K_u = 0.00949 \\ K_I = 0.54 K_u / T_u = 0.314 \end{cases} \tag{18}$$

The instability situation is arrived in step response (Figure 2) due to violation of absolute stability condition of Eq. (15).

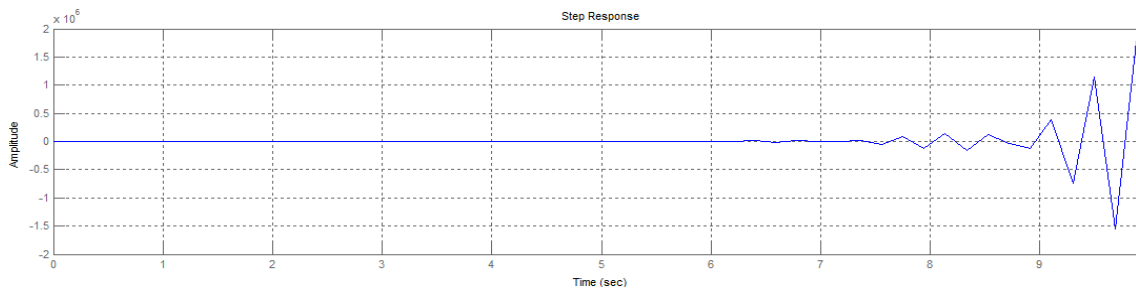


Figure 2. Step response of the system function with gain,  $K = 0.022$ .

### 3 Determination of Speed Controller Gains for Achieving Superior Transient Performance and Sound Stability Margin Under Variable Operating Conditions

The Ziegler-Nichols tuning table does not provide satisfactory transient response and sufficient stability margin as it is not system-specific. Now, more investigation is needed to obtain a better transient response of the system, and relative stability is also to be simultaneously investigated. Various operational conditions under both motor and regenerative modes are taken into account in the following studies so that retuning of PI gains will be done to get superior transient performance and a sound stability margin in comparison to that of the Ziegler-Nichols (conventional) case.

#### 4.1 Gain Selection under Motoring Mode

A battery-based bidirectional converter is controlled to operate the PMDC motor at the desired speed under variable load conditions. A wide range of operating points of the motor (quarter to full load and half to full rated speed operations) is considered for investigations, and these distinct operating points are listed in Table 2. The values of the system matrices vary with variations in operating points, and thus, different transfer functions are to be calculated for different operating points. The transfer function under full load conditions at rated speed operation is already presented in (12). Different transfer functions for the other operating points of Table 2 are calculated and given in (19) to (26). Various intermediate tests are carried out with variable PI gains. The observations are recorded using the step response, the root locus curve and the Bode plots of these transfer functions; only a few of these are shown as reference points in Figures 3-5.

Table 2. Various variables under motor mode.

Speed Condition	Load Condition	$i_a$ (A)	$v_2$ (V)	D (pu)	$i_L$ (A)
Rated Speed(rs)	Full	15.92	240	0.78	71
	Half	7.96	219.45	0.76	33.5
	Quarter	3.98	206.95	0.75	15.96
75% of rated speed(0.75rs)	Full	15.92	190.27	0.73	58.08
	Half	7.96	169.72	0.69	25.9
	Quarter	3.98	159.45	0.67	12.17
50% of rated speed (0.5rs)	Full	15.92	140.54	0.63	42.89
	Half	7.96	118.88	0.56	18.14
	Quarter	3.98	108.61	0.52	8.28

$$G(s) \Big|_{(rs-hl)} = \frac{\hat{\omega}}{\hat{d}} = \frac{-5.463e006.s^2 + 8.178e011.s + 5.049e015}{s^5 + 6092.s^4 + 1.112e007.s^3 + 4.397e009.s^2 + 3.662e011.s + 5.637e012} \quad (19)$$

$$G(s) \Big|_{(rs-ql)} = \frac{\hat{\omega}}{\hat{d}} = \frac{-2.602e006.s^2 + 8.347e011.s + 5.076e015}{s^5 + 6092.s^4 + 1.118e7.s^3 + 4.741e009.s^2 + 3.976e011.s + 6.2e012} \quad (20)$$

$$G(s) \Big|_{(0.75rs-fl)} = \frac{\hat{\omega}}{\hat{d}} = \frac{-9.471e006.s^2 + 7.936e011.s + 5.008e015}{s^5 + 6092.s^4 + 1.131e007.s^3 + 5.532e009.s^2 + 4.697e011.s + 7.494e012} \quad (21)$$

$$G(s) \Big|_{(0.75rs-hl)} = \frac{\hat{\omega}}{\hat{d}} = \frac{-4.223e006.s^2 + 8.251e011.s + 5.06e015}{s^5 + 6092.s^4 + 1.15e007.s^3 + 6.708e009.s^2 + 5.769e011.s + 9.418e012} \quad (22)$$

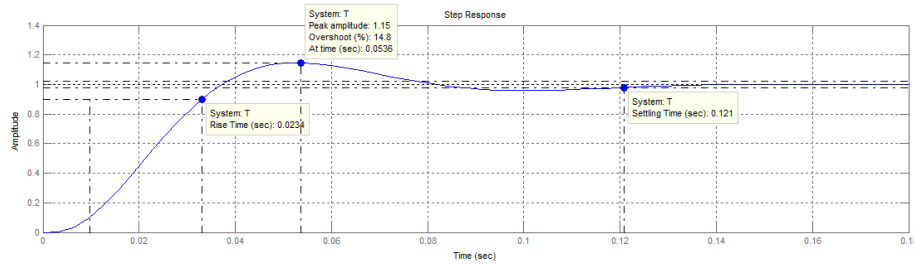


$$G(s) \Big|_{(0.75rs-ql)} = \frac{\hat{\omega}}{\hat{d}} = \frac{-1.984e006.s^2 + 8.383e011.s + 5.081e015}{s^5 + 6092.s^4 + 1.163e007.s^3 + 7.469e009.s^2 + 6.464e011.s + 1.066e013} \tag{23}$$

$$G(s) \Big|_{(0.5rs-fl)} = \frac{\hat{\omega}}{\hat{d}} = \frac{-6.994e006.s^2 + 8.085e011.s + 5.033e015}{s^5 + 6092.s^4 + 1.194e007.s^3 + 9.345e009.s^2 + 8.174e011.s + 1.373e013} \tag{24}$$

$$G(s) \Big|_{(0.5rs-hl)} = \frac{\hat{\omega}}{\hat{d}} = \frac{-2.958e006.s^2 + 8.327e011.s + 5.073e015}{s^5 + 6092.s^4 + 1.248e007.s^3 + 1.268e010.s^2 + 1.122e012.s + 1.919e013} \tag{25}$$

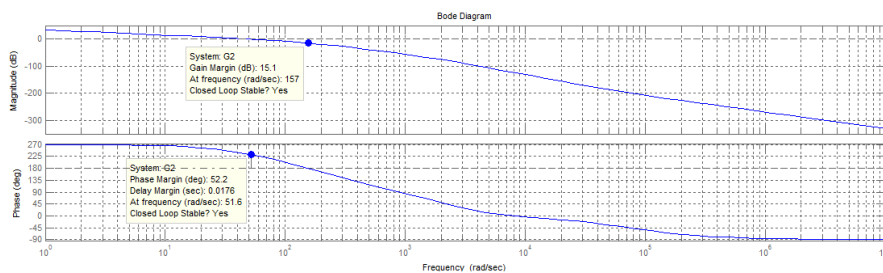
$$G(s) \Big|_{(0.5rs-ql)} = \frac{\hat{\omega}}{\hat{d}} = \frac{-1.35e006.s^2 + 8.423e011.s + 5.089e015}{s^5 + 6092.s^4 + 1.287e007.s^3 + 1.5e010.s^2 + 1.333e012.s + 2.299e013} \tag{26}$$



(a) Step response with allied specifications

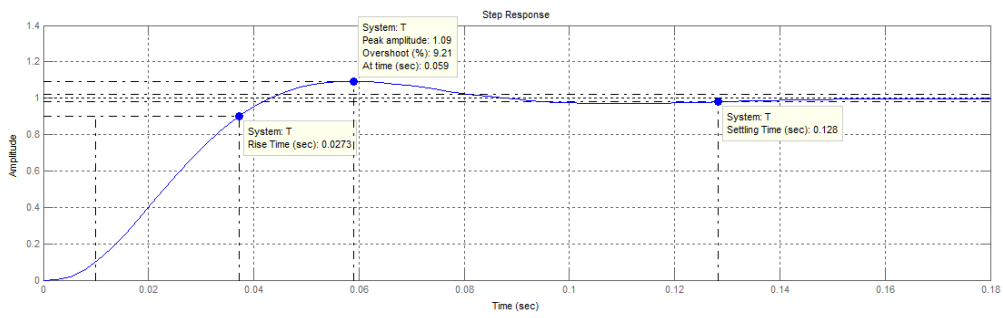


(b) Root locus diagram with dominant pole-pair location

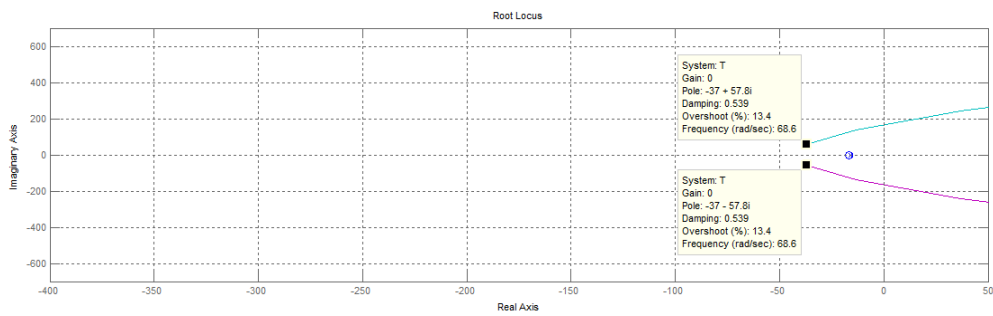


(c) Bode plot with stability margins

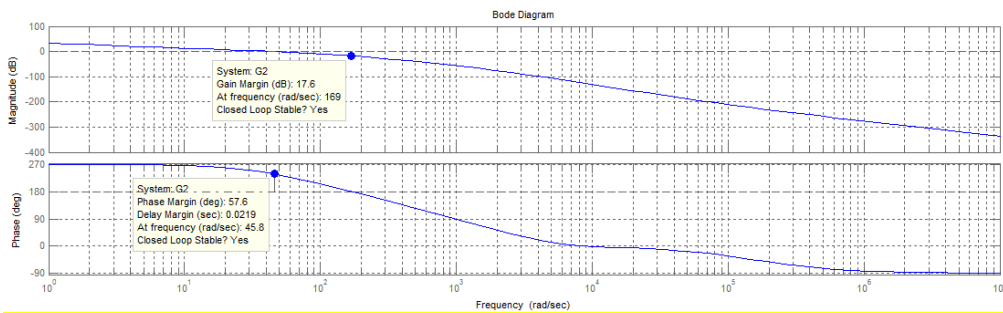
Figure 3. Various performance specifications under fully loading and rated speed conditions with  $K_P=0.003$ ,  $K_I=0.05$ .



(a) Step response with allied specifications

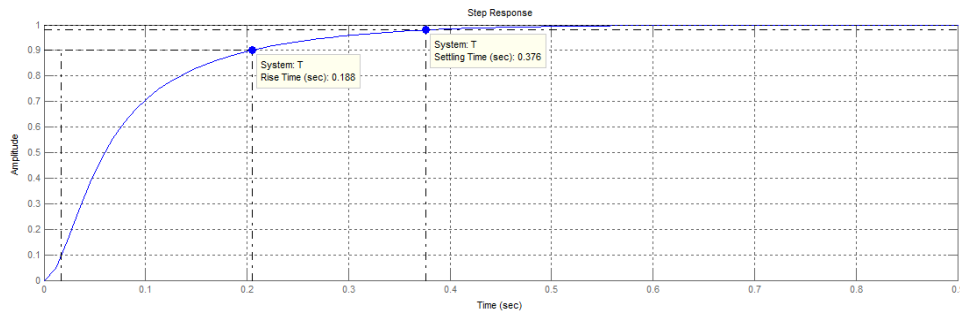


(b) Root locus diagram with dominant pole-par location

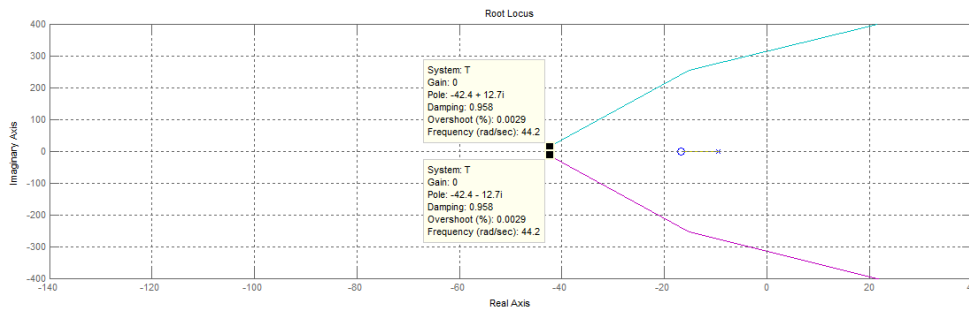


(c) Bode plot with stability margins

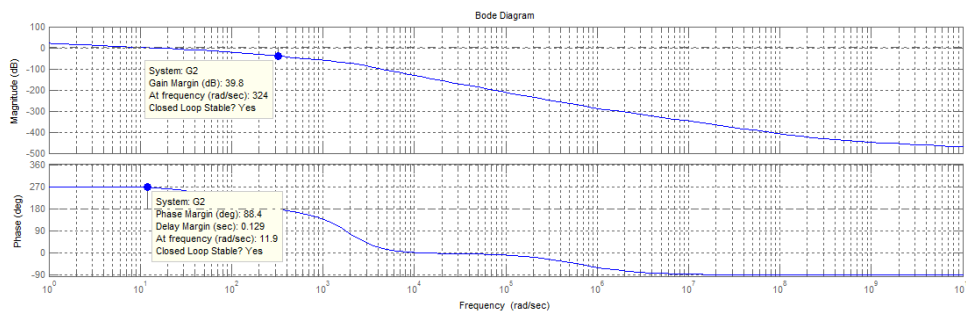
Figure 4. Various performance specifications under half loading and rated speed condition with  $K_P=0.003$ ,  $K_I=0.05$ .



(a) Step response with allied specifications



(b) Root locus diagram with dominant pole-pair location



(c) Bode plot with stability margins

Figure 5. Various performance specifications under quarter loading and 50% of rated speed condition with  $K_P=0.003, K_I=0.05$ .

From above said rigorous investigations, best possible tuning values of PI gains for individual speed case are noted in Table 3. Finally, common PI gains and associated performance criteria (both are specified in last row of Table 3) are decided for speed control loop to achieve best possible dynamic performances under variable speed conditions in motoring mode.

Table 3. Various variables under motor mode.

Speed Condition	$M_p(\%)$	$t_r(s)$	$t_s(s)$	GM(dB)	PM( $^\circ$ )	Best Possible PI gains
Rated Speed(rs)	nil	0.157	0.478	16.3	64.4	$K_p=0.003, K_i=0.02$
75% of rated speed(0.75rs)	1.53	0.0592	0.187	21.9	66.4	$K_p=0.003, K_i=0.05$
50% of rated speed (0.5rs)	1.74	0.11	0.195	30.6	69.3	$K_p=0.003, K_i=0.07$
<b>Common Criteria &amp; Gains</b>	<b>&lt;5%</b>	<b>&lt;0.5</b>	<b>&lt;1.0</b>	<b>&gt;15</b>	<b>&gt;60</b>	<b><math>K_p=0.003, K_i=0.03</math></b>

### 4.1 Gain Selection under Regenerative Mode

During the regenerating period, the voltage at the input terminals of the machine is to be adjusted by controlling the bidirectional converter. Here, the back EMF exceeds the input voltage to reverse the current flow, i.e., motor power is feeding back to the battery through a bidirectional converter.

In this mode, variables at different operating points of the machine under the study of this paper are listed in Table 4.

Table 4. Various variables under regenerative mode.

Speed Condition	Load Condition	$i_a$ (A)	$v_2$ (V)	D (pu)	$i_L$ (A)
Rated Speed(rs)	Full	15.92	157.82	0.67	48.18
	Half	7.96	178.36	0.70	27.23
	Quarter	3.98	188.64	0.72	14.39
75% of rated speed(0.75rs)	Full	15.92	108.09	0.51	32.99
	Half	7.96	128.63	0.59	19.63
	Quarter	3.98	138.91	0.62	10.59
50% of rated speed (0.5rs)	Full	15.92	58.36	0.10	17.81
	Half	7.96	78.9	0.33	12.04
	Quarter	3.98	89.18	0.41	6.8

The small signal models under the mode are given in (27). The corresponding transfer functions are expressed in (28) to (36). The system matrices of (27) are same as of (10) except the change of sign in the term ' $I_L/C_2$ ' for the matrix of ' $\hat{d}$ '.

$$\begin{aligned}
 \begin{cases} p(-\hat{i}_L) \\ p(\hat{v}_1) \\ p(-\hat{i}_a) \\ p(\hat{v}_2) \\ p(\hat{\omega}) \end{cases} &= \begin{bmatrix} 0 & 1/L_1 & 0 & -(1-D)/L_1 & 0 \\ -1/C_1 & -1/R_1 C_1 & 0 & 0 & 0 \\ 0 & 0 & -R_a/L_2 & 1/L_2 & -k/L_2 \\ (1-D)/C_2 & 0 & -1/C_2 & 0 & 0 \\ 0 & 0 & k/J & 0 & -B/J \end{bmatrix} \begin{bmatrix} -\hat{i}_L \\ \hat{v}_1 \\ -\hat{i}_a \\ \hat{v}_2 \\ \hat{\omega} \end{bmatrix} + \begin{bmatrix} V_2/L_1 \\ 0 \\ 0 \\ I_L/C_2 \\ 0 \end{bmatrix} \begin{bmatrix} \hat{d} \end{bmatrix} \\
 [p(\hat{y})] &= [0 \ 0 \ 0 \ 0 \ 1] \begin{bmatrix} \hat{i} \\ \hat{v}_1 \\ \hat{i}_a \\ \hat{v}_2 \\ \hat{\omega} \end{bmatrix}
 \end{aligned} \tag{27}$$

$$G(s) \Big|_{(rs-fl)} = \frac{\hat{\omega}}{\hat{d}} = \frac{7.827e006.s^2 + 8.972e011.s + 5.18e015}{s^5 + 6092.s^4 + 1.165e007.s^3 + 7.605e009.s^2 + 6.588e011.s + 1.089e013} \tag{28}$$

$$G(s) \Big|_{(rs-hl)} = \frac{\hat{\omega}}{\hat{d}} = \frac{4.435e006.s^2 + 8.767e011.s + 5.145e015}{s^5 + 6092.s^4 + 1.141e007.s^3 + 6.16e009.s^2 + 5.27e011.s + 8.522e012} \tag{29}$$

$$G(s) \Big|_{(rs-ql)} = \frac{\hat{\omega}}{\hat{d}} = \frac{2.348e006.s^2 + 8.642e011.s + 5.124e015}{s^5 + 6092.s^4 + 1.132e007.s^3 + 5.609e009.s^2 + 4.767e011.s + 7.62e012} \tag{30}$$

$$G(s)_{(0.75rs-fl)} = \frac{\hat{\omega}}{\hat{d}} = \frac{5.379e006.s^2 + 8.827e011.s + 5.156e015}{s^5 + 6092.s^4 + 1.289e007.s^3 + 1.514e010.s^2 + 1.346e012.s + 2.321e013} \quad (31)$$

$$G(s)_{(0.75rs-hl)} = \frac{\hat{\omega}}{\hat{d}} = \frac{3.201e006.s^2 + 8.697e011.s + 5.135e015}{s^5 + 6092.s^4 + 1.22e007.s^3 + 1.097e010.s^2 + 9.658e011.s + 1.64e013} \quad (32)$$

$$G(s)_{(0.75rs-ql)} = \frac{\hat{\omega}}{\hat{d}} = \frac{1.727e006.s^2 + 8.609e011.s + 5.121e015}{s^5 + 6092.s^4 + 1.197e007.s^3 + 9.545e009.s^2 + 8.356e011.s + 1.406e013} \quad (33)$$

$$G(s)_{(0.5rs-fl)} = \frac{\hat{\omega}}{\hat{d}} = \frac{2.904e006.s^2 + 8.678e011.s + 5.131e015}{s^5 + 6092.s^4 + 1.854e007.s^3 + 4.96e010.s^2 + 4.488e012.s + 7.961e013} \quad (34)$$

$$G(s)_{(0.5rs-hl)} = \frac{\hat{\omega}}{\hat{d}} = \frac{1.963e006.s^2 + 8.622e011.s + 5.122e015}{s^5 + 6092.s^4 + 1.493e007.s^3 + 2.757e010.s^2 + 2.48e012.s + 4.356e013} \quad (35)$$

$$G(s)_{(0.5rs-ql)} = \frac{\hat{\omega}}{\hat{d}} = \frac{1.166e006.s^2 + 9.014e011.s + 5.378e015}{s^5 + 6092.s^4 + 1.398e007.s^3 + 2.179e010.s^2 + 1.953e012.s + 3.585e013} \quad (36)$$

Table 5 shows that the best possible gains at different speeds under regenerative mode. The common PI gains and performance criteria under regenerative mode are specified at the end of Table 5.

Table 5. Various variables under regenerative mode.

Speed Condition	M <sub>p</sub> (%)	t <sub>r</sub> (s)	t <sub>s</sub> (s)	GM(dB)	PM(°)	Best Possible PI gains
Rated Speed(rs)	nil	0.175	0.414	22.7	77.6	K <sub>p</sub> =0.003, K <sub>i</sub> =0.03
75% of rated speed(0.75rs)	1.65	0.11	0.194	30.9	69.5	K <sub>p</sub> =0.003, K <sub>i</sub> =0.05
50% of rated speed (0.5rs)	1.11	0.288	0.512	43.8	72.1	K <sub>p</sub> =0.003, K <sub>i</sub> =0.1
<b>Common Criteria &amp; Gains</b>	<b>&lt;5%</b>	<b>&lt;0.8</b>	<b>&lt;1.5</b>	<b>&gt;20</b>	<b>&gt;60</b>	<b>K<sub>p</sub>=0.003, K<sub>i</sub>=0.05</b>

#### 4.1 Selection of Single PI Controller Gains Considering both Motoring and Regenerative Mode

The gain combinations of the motor mode (last row of Table 3) differ from those of the regenerative mode (last row of Table 5). A compromise solution must therefore be found, i.e. the lowest possible compromise criteria must be observed. Various intermediate tests are again carried out in order to obtain the best possible PI gain combination, regardless of the type of operating mode. The best possible PI gains in terms of better operating behaviour are listed in Table 6. The guidelines for transient behaviour and relative stability are also listed in Table 6 as general performance criteria for speed control loops in each operating mode.

Table 6. Performance specifications with best possible PI gains under both modes.

Speed Condition	M <sub>p</sub> (%)	t <sub>r</sub> (s)	t <sub>s</sub> (s)	GM(dB)	PM(°)	Best Possible PI gains
<b>Common Criteria &amp; Gains</b>	<b>&lt;10%</b>	<b>&lt;0.9</b>	<b>&lt;1.8</b>	<b>&gt;15</b>	<b>&gt;50</b>	<b>K<sub>p</sub>=0.003, K<sub>i</sub>=0.04</b>

The transient and stability performances under both modes are compared between selected gains (the common gain in Table 6) and conventional gains (Eq. 18). The comparison is given in Tables 7 and 8 under motor and regenerative modes, respectively.

Notable points are observed from the performance parameter values in Tables 7 and 8 for wide operations of the drive system as,

- i) In both operational cases, the proposed gains significantly improve the stability margin.
- ii) In many operational cases, the oscillatory behavior of the step response is noticed in conventional cases.
- iii) Peak overshoot in conventional case is very high in almost all cases under both modes. So, it is not acceptable for practical application under variable operating conditions.
- iv) Though the rise time in the conventional case is superior to that of the proposed case, it is not acceptable due to the high value of the maximum overshoot, as already stated in (iii).
- v) The setting time in the proposed case is satisfactory for the drive system.
- vi) The charging process (regenerative mode) is sluggish in comparison to the discharging action of the battery (motor mode).

Therefore, the gains proposed in Table 6 can be said to be the better option compared to the gains obtained from the Ziegler-Nichols tuning table. The validation of the superiority of the obtained gains is also performed using physical system modelling in MATLAB-SIMULINK software platform.

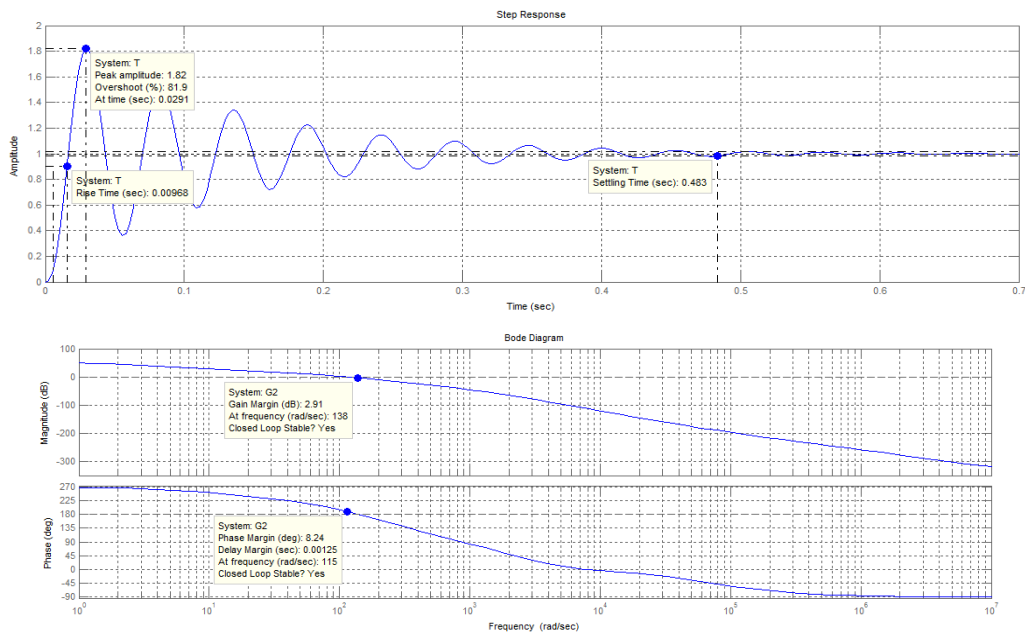
Table 7. Comparative transient and relative stability performances between conventional (Eq.18) and proposed (last row of Table 6) tuned gains under motor mode.

Operating Condition	Conventional Case ( $K_P=0.00949$ , $K_I=0.314$ )					Proposed Case ( $K_P=0.003$ , $K_I=0.04$ )				
	$M_p(\%)$	$t_r(s)$	$t_s(s)$	GM (dB)	PM( $^\circ$ )	$M_p(\%)$	$t_r(s)$	$t_s(s)$	GM (dB)	PM( $^\circ$ )
rs-fl	81.9	0.00968	0.483	2.91	8.24	9.48	0.0246	0.133	15.5	56.2
rs-hl	70.5	0.0105	0.288	5.41	14.3	3.86	0.0291	0.156	18	62.1
rs-ql	65	0.0109	0.242	6.79	17.3	1.18	0.0323	0.173	19.4	65.2
0.75rs-fl	55.1	0.0123	0.176	9.75	23.1	nil	0.042	0.209	22.3	71.9
0.75rs-hl	46	0.0141	0.16	13.2	28.8	nil	0.0645	0.251	25.7	78.8
0.75rs-ql	41.8	0.0153	0.137	15.2	31.6	nil	0.0914	0.276	27.7	82.4
0.5rs-fl	34.1	0.0186	0.152	19.3	37.2	nil	0.148	0.339	31.7	89.9
0.5rs-hl	26	0.0235	0.139	24.7	43.6	nil	0.216	0.442	37.2	94.1
0.5rs-ql	22.5	0.0269	0.151	27.7	46.8	nil	0.26	0.513	40.1	95.2

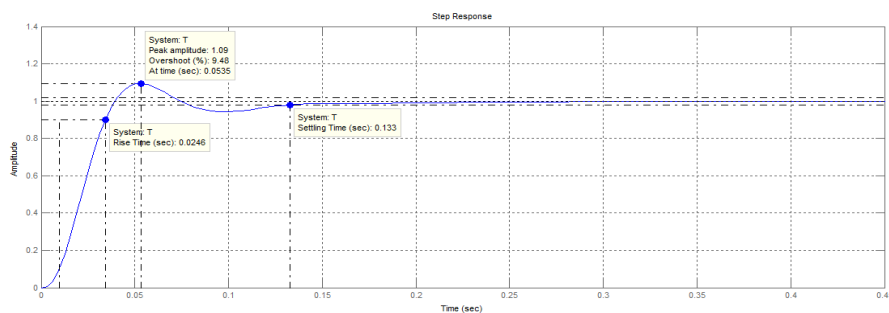
Table 8. Comparative transient and relative stability performances between conventional (Eq.18) and proposed (last row of Table 6) tuned gains under regenerative mode.

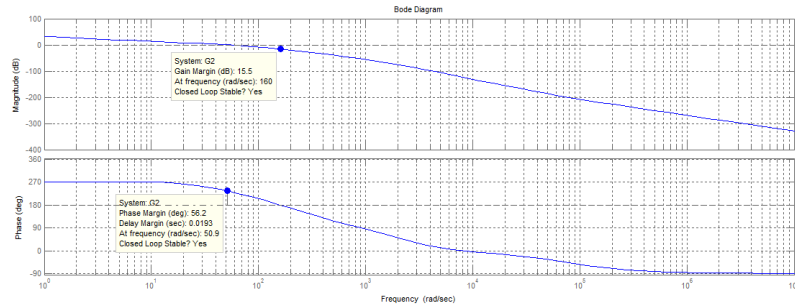
Operating Condition	Conventional Case ( $K_p=0.00949$ , $K_i=0.314$ )					Proposed Case ( $K_p=0.003$ , $K_i=0.04$ )				
	$M_p(\%)$	$t_r(s)$	$t_s(s)$	GM (dB)	PM( $^\circ$ )	$M_p(\%)$	$t_r(s)$	$t_s(s)$	GM (dB)	PM( $^\circ$ )
rs-fl	41.6	0.0153	0.137	15.4	31.8	nil	0.0922	0.229	27.9	82.5
rs-hl	50.2	0.0131	0.178	11.6	26.1	nil	0.0496	0.229	24.1	75.2
rs-ql	54.9	0.0122	0.175	9.86	23.2	nil	0.0417	0.209	22.4	71.7
0.75rs-fl	22.5	0.0268	0.151	27.8	46.7	nil	0.259	0.512	40.2	95.2
0.75rs-hl	30	0.0207	0.127	22.1	40.4	nil	0.179	0.385	34.5	92.1
0.75rs-ql	33.8	0.0187	0.152	19.6	37.4	nil	0.149	0.341	32	89.3
0.5rs-fl	3.95	0.0797	0.228	48.9	67.1	nil	0.878	1.58	61.2	92.7
0.5rs-hl	11.4	0.0452	0.16	38.5	57.5	nil	0.487	0.898	50.9	94.4
0.5rs-ql	14.5	0.0357	0.129	33.9	54.2	nil	0.387	0.728	46.3	96

Figure 6 - 11 shows comparative transient response and corresponding relative stability limits under various operating conditions.



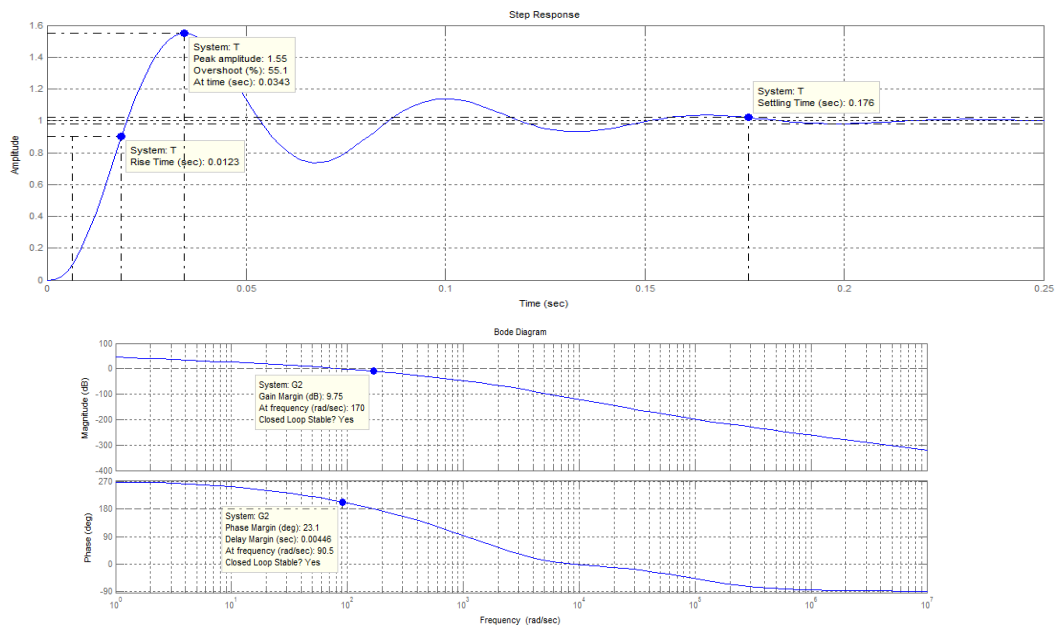
(a) Conventional case





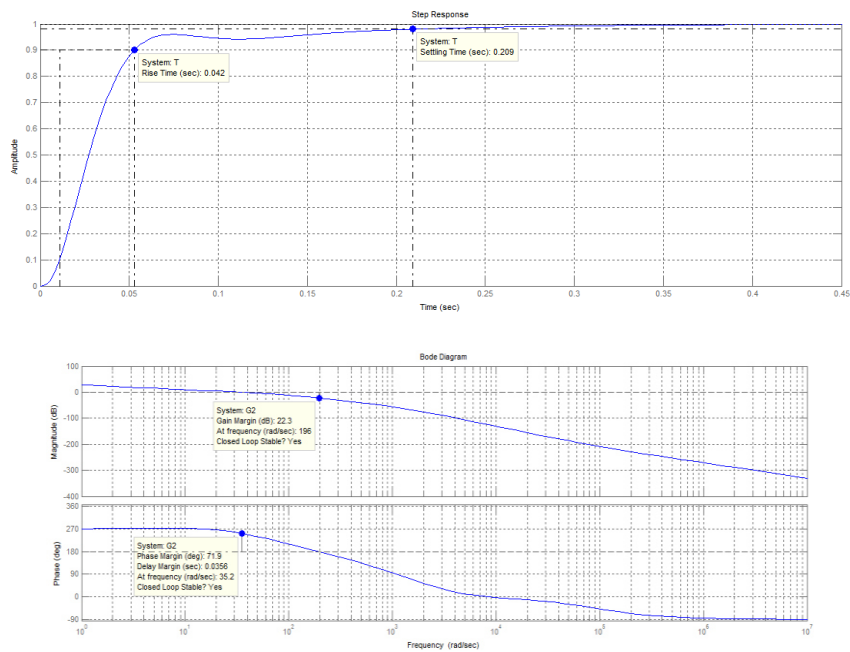
(b) Proposed case

Figure 6. Comparative transient, relative stability parameters in full-loading and rated speed condition under motoring mode.



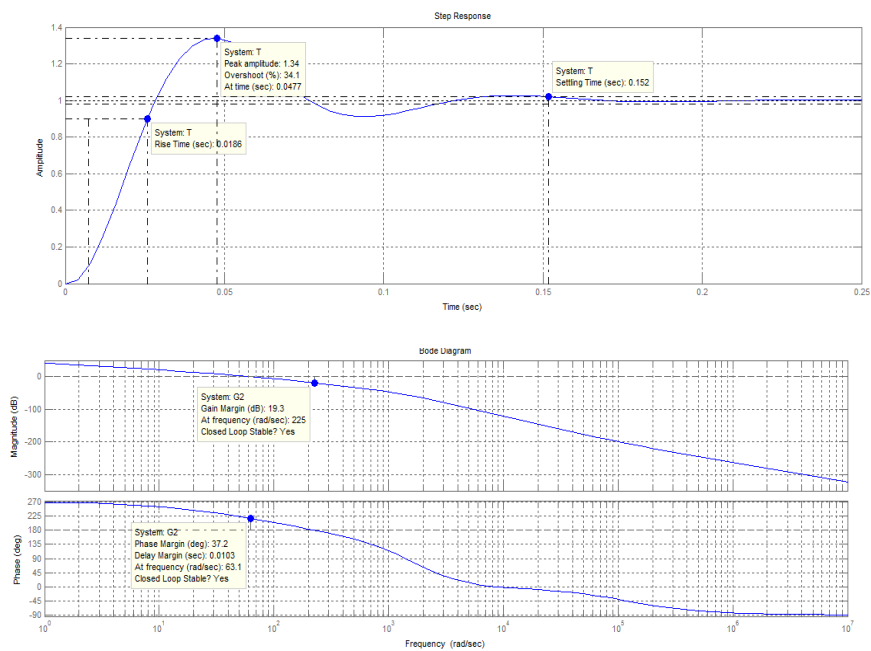
(a) Conventional case



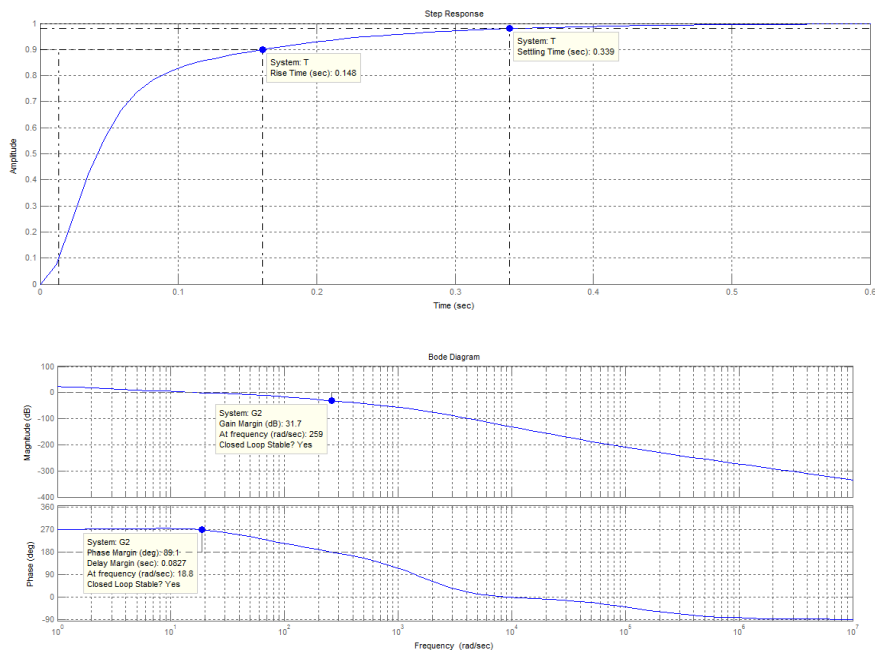


(b) Proposed case

Figure 7. Comparative transient, relative stability parameters in full-loading and 75% of rated speed condition under motoring mode.

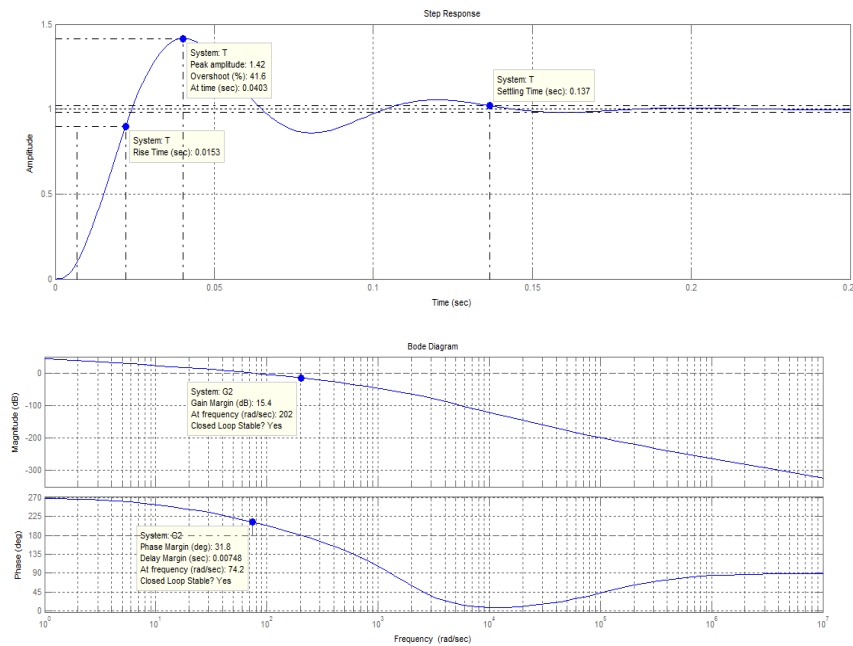


(a) Conventional case

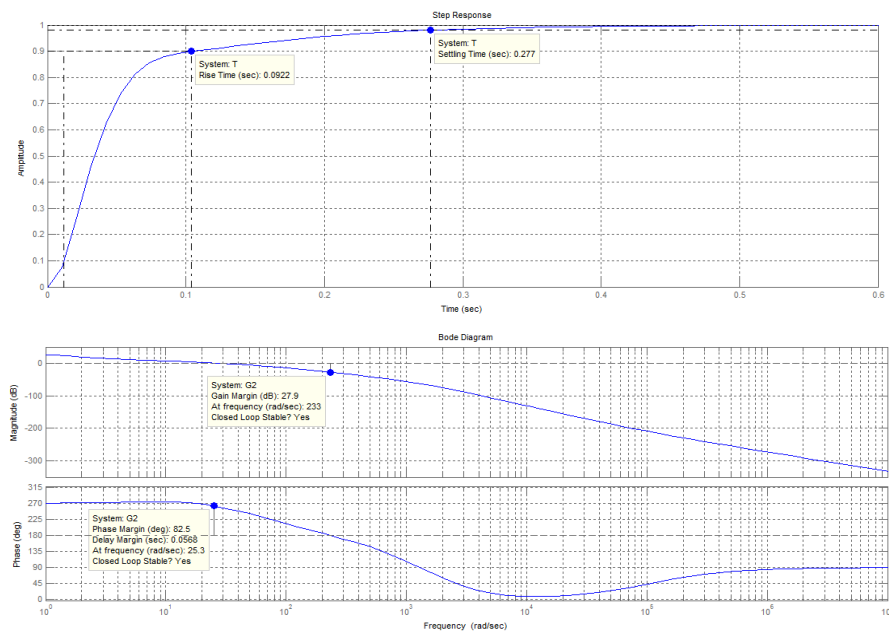


(b) Proposed case

Figure 8. Comparative transient, relative stability parameters in full-loading and 50% of rated speed condition under motoring mode.

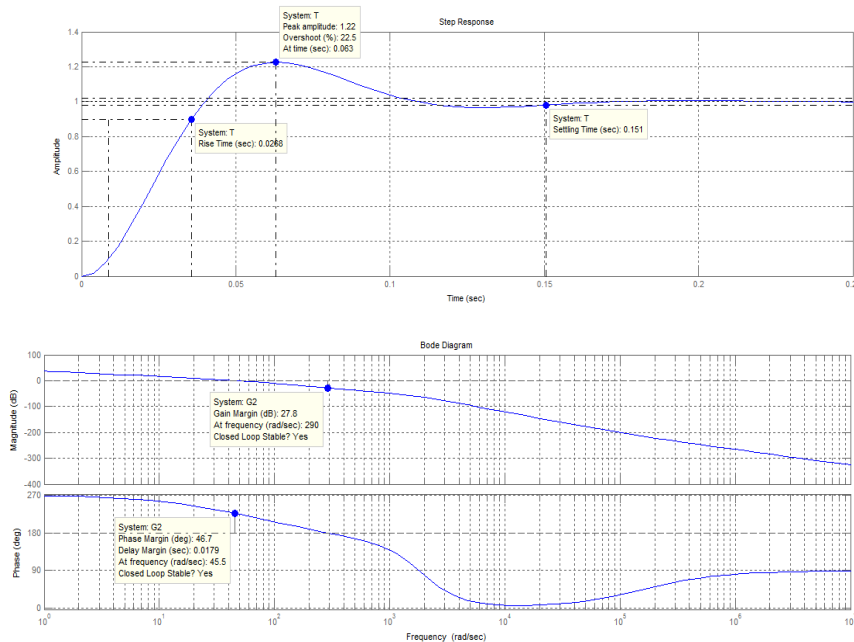


(a) Conventional case

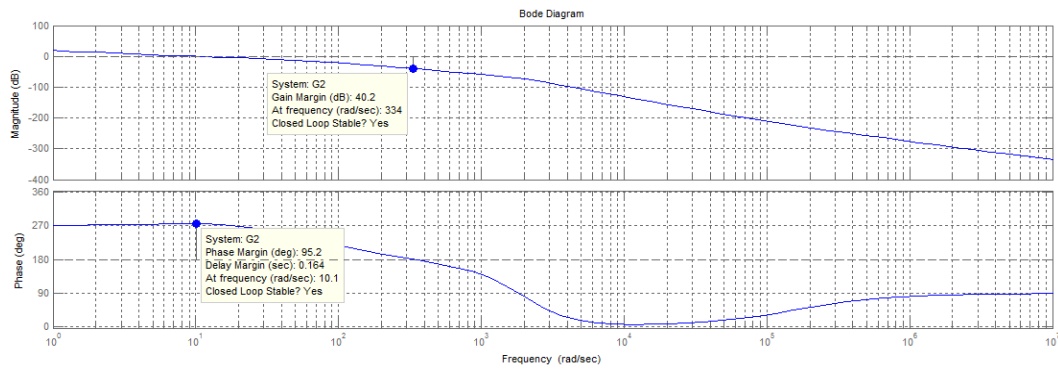


(b) Proposed case

Figure 9. Comparative transient, relative stability parameters in full-loading and rated speed condition under regenerative mode.

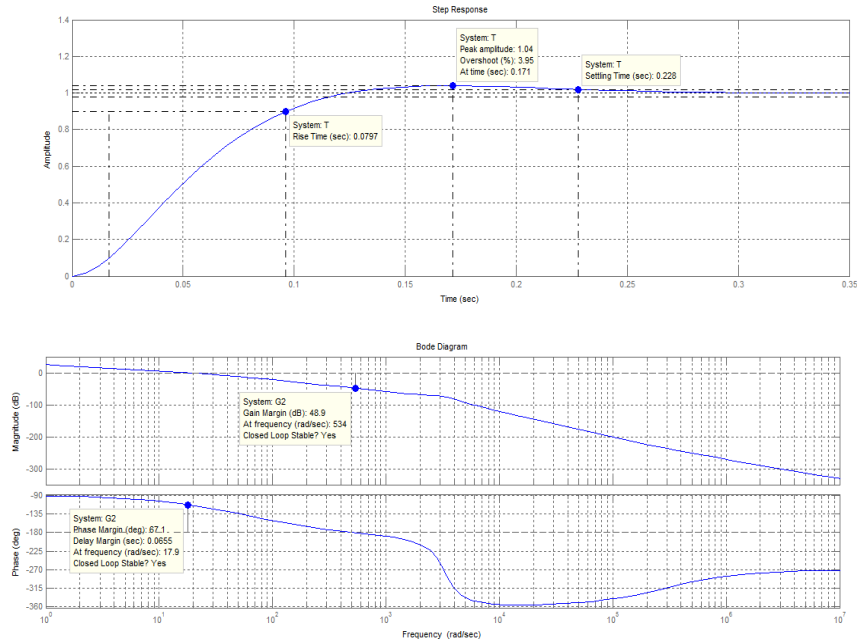


(a) Conventional case

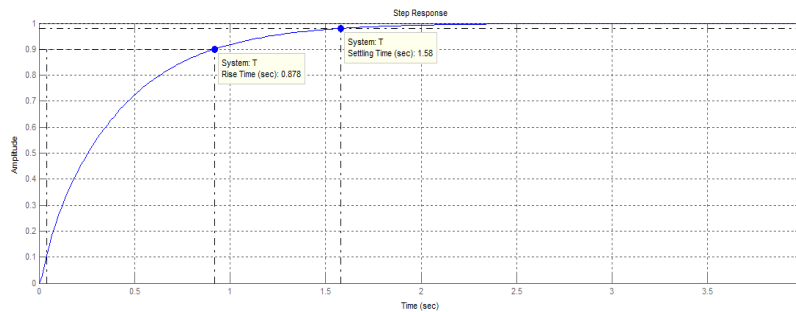


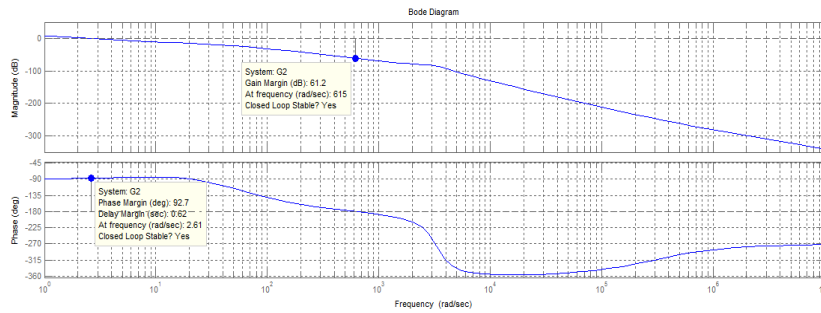
(b) Proposed case

Figure 10. Comparative transient, relative stability parameters in full-loading and 75% of rated speed condition under regenerative mode.



(a) Conventional case





(b) Proposed case

Figure 11. Comparative transient, relative stability parameters in full-loading and 50% of rated speed condition under regenerative mode.

### 4 Large Signal Model Analysis

The effect of large load torque variation is not discussed in the previous discussions, which is an important issue in terms of practical implementation. Thus, the large signal model analysis is provided in the subsequent discussions. In this regard, the mathematical formulation is given in (37), which is derived from (9). The stability of the model is analysed under large load torque variations (20%). In this context, the phase portraits of the conventional and the proposed model are shown to compare the relative stability performance under large variations of the load torque. From the plots shown in Fig. 12, the following observations can be derived:

- i. The damping effect of the proposed tuned model is superior as it significantly suppresses the speed oscillation under large load torque variations,
- ii. The current variations are also significantly less in the proposed model than in the in the conventional case during the dynamic operation,
- iii. The speed deviation during large is opposite in the case of regenerative action than in the in the motoring case for both models.

Thus, the proposed tuning process provides superior stability from the large signal analysis.

$$\begin{aligned}
 \frac{d}{dt} I_a(t) &= -\frac{R_a}{L_2} I_a(t) - \frac{k}{L_2} \omega(t) + \frac{V_2(t)}{L_2} \\
 \frac{d}{dt} V_2(t) &= \frac{(1-D-\hat{D})}{C_2} I_L - \frac{I_a(t)}{C_2} \\
 \frac{d}{dt} \omega(t) &= \frac{k}{J} I_a(t) - \frac{B}{J} \omega(t) - \frac{T_L(t)}{J}
 \end{aligned}
 \tag{37}$$

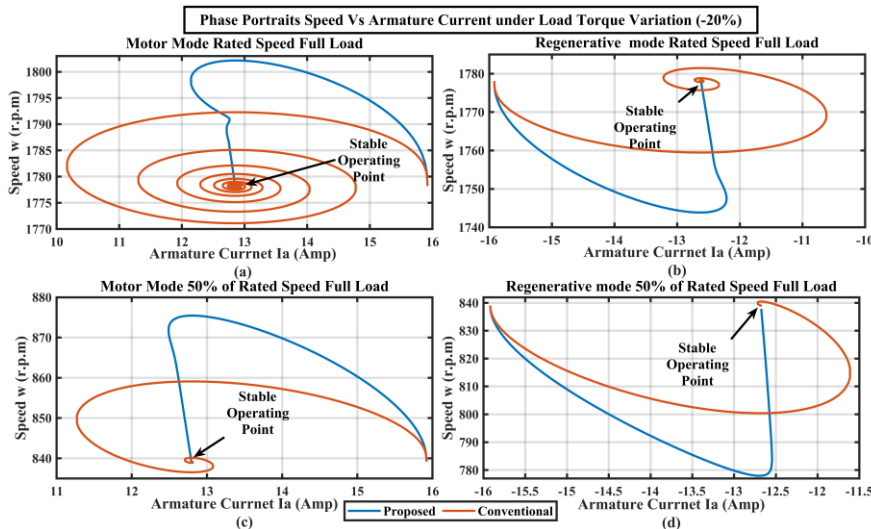


Figure 12. Phase portraits under large load torque variations.

## 5 Simulation Study

In this section, the dynamic response of the speed control loop is evaluated using a SIMULINK software-based model of a physical system. The parameters of the physical system are already given in Table 1. In Fig. 13, comparative dynamic speed responses between conventional gains ( $K_P = 0.00949$ ,  $K_I = 0.314$ ) and proposed gains ( $K_P = 0.003$ ,  $K_I = 0.04$ ) under motor mode are presented subject to speed conditions:

From simulation time ( $t$ ) = 0 sec to  $t = 0.6$  sec, the motor is operated at 50% of its rated speed, and after  $t = 0.6$  sec, it is operated at the rated speed condition.

It is found to exhibit oscillatory behaviour and, thus, a lower relative stability of speed response in the conventional case than that in the proposed case. Therefore, it agrees with the previous analysis of Section 4.

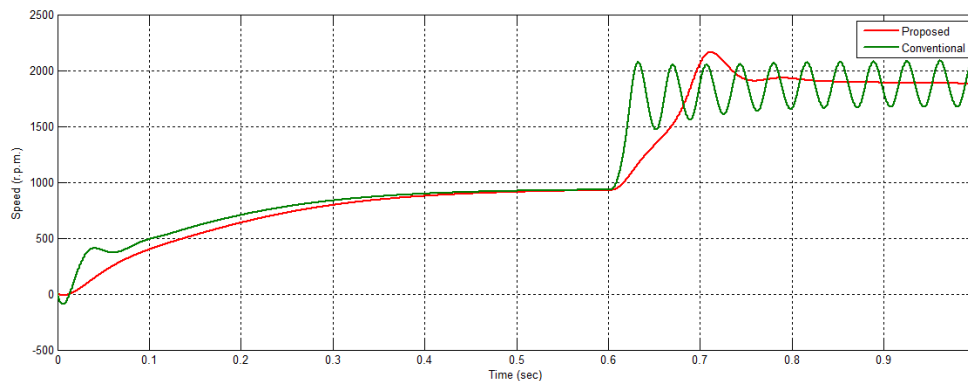


Figure 13. Comparative dynamic speed responses between proposed and conventional cases

Next, the dynamic responses of both cases are shown in Figure 14 under regenerative mode, subject to the same speed conditions as in Figure 13 (mentioned just above). It is found that responses are comparatively sluggish in the regenerative/charging case (Figure 14) than in the motor/discharge mode (Figure 13). It also agrees with the analysis of this paper (section 4). In Figure 13, the response in the proposed case is smoother than the conventional one.

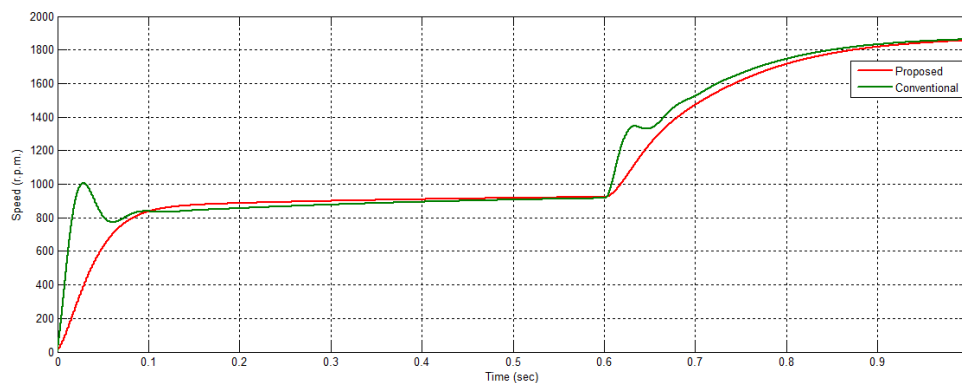


Figure 14. Comparative dynamic speed responses under regenerative mode.

In Figure 15, the dynamic speed responses in the fully-rated condition are compared subject to input supply voltage variation under motor mode as follows:

From simulation time ( $t$ ) = 0 sec to  $t = 0.6$  sec, the motor is operated at rated speed with a battery voltage of 52.15 V, and at  $t = 0.6$  sec, the voltage is suddenly changed to 42.15 V.

Figure 15 shows more oscillatory behavior in the conventional case when the drive system is subjected to input voltage variation.

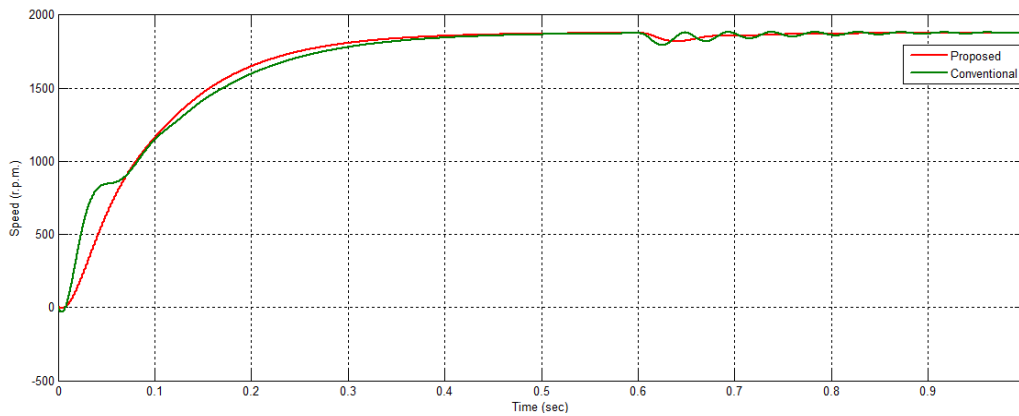


Figure 15. Comparative dynamic speed responses under variation of supply conditions.

The absolute stability condition of gain is verified in this simulation platform, and the related response is shown in Fig. 16. The obtained speed response at the rated condition is presented under a sudden change of proportional gain at  $t = 0.6$  sec from the value of 0.003 to 0.03. It is noticed that the desired (reference) speed response is not maintained after  $t = 0.6$  sec due to a violation of the gain condition as per (18).

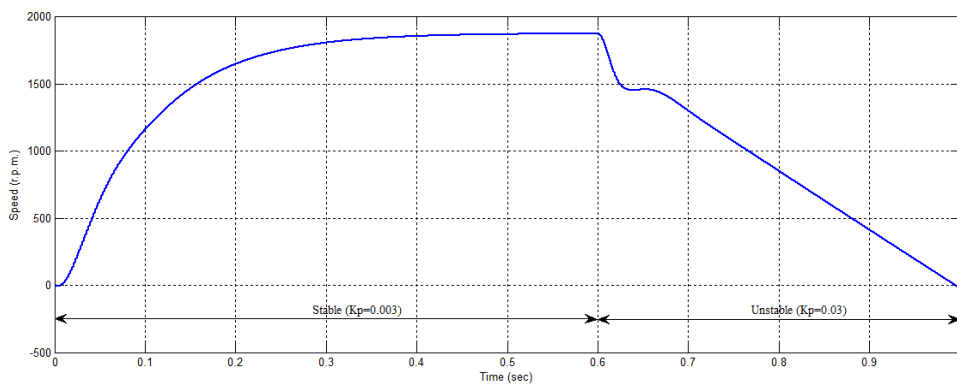


Figure 16. Desired speed Response for  $K_p = 0.003$  up to simulation time = 0.6 sec, then failure in the response for changed value of  $K_p = 0.03$ .

Thus, various results of the simulation study on the physical system model demonstrate the dynamic performances of PMDC machine-based drive systems in line with the analysis in the previous section.

## 7 Experimental Performance

The set-up for carrying out the experimental studies is shown in Figure 17. Studies are carried out on speed and load torque fluctuations. The results confirm the various analyses in the paper. The speed reference is changed from 1480 rpm to 1400 rpm in Figure 18 and 19 for motoring and regenerative modes, respectively. The speed tracking performance under this dynamic operation is satisfactory for the proposed tuning method. Here, Figure 18 and 19 also present the dynamic variations of armature current and input terminal voltage in the speed change operations. The load torque variation case studies are performed under 75% of the rated speed operation. Here, the machine is operated at a speed of 1400 rpm. For a 5% change in load torque, the obtained speed, armature current, and input voltage are shown in Figure 20 and 21 for motoring and regenerative modes. Here, the performance is satisfactory for the speed control loop with the proposed tuning method.



Figure 17. Experimental platform.

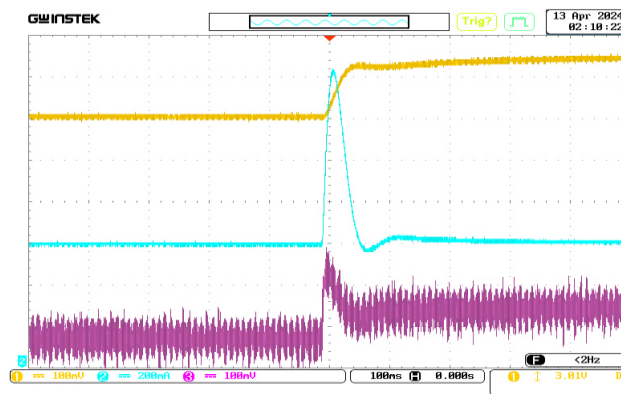


Figure 18. Variables under motor mode at 75% of rated speed and full load with 5% increase of reference speed (1400 rpm).

Yellow (top plot):- Speed (scale- 1:470) change from 1400 rpm to 1480 rpm,  
 Blue (middle plot):- Aarmature current (scale- 1:5) change from 15.7 A to 15.6 A,  
 Pink (bottom plot):- Aarmature voltage (scale- 1:100) change from 190 V to 197 V.

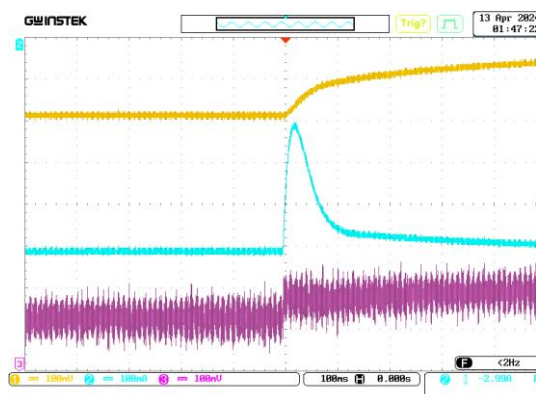


Figure 19. Variables under regenerative mode at 75% of rated speed and full load with 5% increase of reference speed (1400 rpm).

Yellow (top plot):- Speed (scale- 1:470) change from 1400 rpm to 1480 rpm,  
 Blue (middle plot):- Aarmature current (scale- 1:5) change from 15.9 A to 15.8 A,  
 Pink (bottom plot):- Aarmature voltage (scale- 1:100) change from 108 V to 115.6 V.



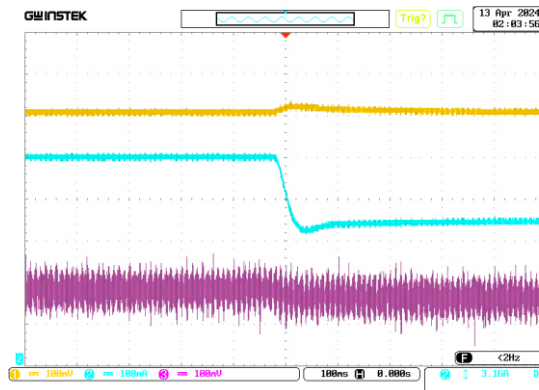


Figure 20. Variables under motor mode at 75% of rated speed and full load with 5% load torque reduction.  
 Yellow (top plot):- Speed (scale- 1:470) at 1400 rpm,  
 Blue (middle plot):- Armature current (scale- 1:5) change from 15.7 A to 14.9 A,  
 Pink (bottom plot):- Armature voltage (scale- 1:100) change from 190 V to 188 V.

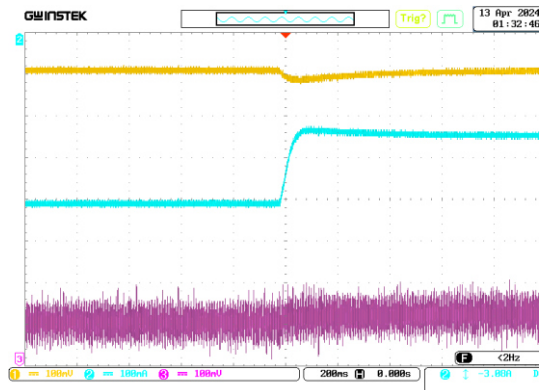


Figure 21. Variables under regenerative mode at 75% of rated speed and full load with 5% load torque reduction.  
 Yellow (top plot):- Speed (scale- 1:470) at 1400 rpm,  
 Blue (middle plot):- Armature current (scale- 1:5) change from 15.9 A to 15.1 A,  
 Pink (bottom plot):- Armature voltage (scale- 1:100) change from 108 V to 110 V.

## 8 Conclusion

In this paper, the dynamic performance of the speed control loop of a battery-powered PMDC machine is analysed in both motor and generator mode. The Ziegler-Nichols tuning chart is used to design PI gains for the system. But this conventional process does not provide satisfactory transient performance and relative stability. Therefore, the redesigning of speed controller is done based on rigorous investigations of system performances under variable operating conditions. Finally, a single pair of PI gains is chosen, irrespective of the type of mode. The designed gains provide improved transient performance and a significantly stronger stability margin for the speed loop, and in this respect, comparative analysis is done. The model of the physical system in the MATLAB-SIMULINK software platform is prepared, and the performance of the proposed gains is validated. The responses of the proposed cases are compared with those of the conventional cases to justify the superiority of the proposed approach. Finally, a large signal stability analysis affirms the robust performance of the speed control loop of the drive system with the proposed controller design. The experimental studies in the proposed case show the practical implementation of the PMDC drive system.

## Acknowledgement

Authors have no conflict of interest relevant to this article.

## References

- [1] A. Senthilnathan, R. Manohar, J. Mohanavel, AK. OmeshHeman, RK. Saravana, "Smart Hybrid Electric Vehicle", *IEEE int conf on Innovations in Green Energy and Healthcare Technologies*. 2017, 01-06.
- [2] H. Zakaria, M. Hamid, EM. Abdellatif, A. Imane, "Recent Advancements and Developments for Electric Vehicle Technology" *2019 International Conference of Computer Science and Renewable Energies (ICCSRE)*, 2019, DOI: 10.1109/ICCSRE.2019.8807726.
- [3] CC. Chan, "The state of the art of electric, hybrid, and fuel cell vehicles", *Proc. IEEE*, 2007, 95(4), 704–718.
- [4] L. Ren, Z. Song, C. Mao, F. Liu, "Multitime scale coordinated scheduling for electric vehicles considering photovoltaic/wind/battery generation in microgrid", *Int Trans Electr Energ Syst*. 2019; 29: e2821. <https://doi.org/10.1002/2050-7038.2821>.
- [5] T. Rawat, KR. Niazi, N. Gupta, S. Sharma, "Impact assessment of electric vehicle charging/discharging strategies on the operation management of grid accessible and remote microgrids" *Int J of Energy research*, 2019, <https://doi.org/10.1002/er.4882>.
- [6] Z. Wang, S. Wang, "Grid power peak shaving and valley filling using vehicle-to-grid systems" *IEEE Trans Pow Deliv*, 2013, 28, 1822-9.
- [7] PT. Krein, MA. Fasugba, "Vehicle-to-grid power system services with electric and plug-in vehicles based on flexibility in unidirectional charging" *CES Trans Electrical Machines Sys*, 2017, 1(1), 26-36.
- [8] SMB. Billah, KK. Islam, "Regenerative braking characteristics of PMDC motor by applying different armature voltage" *2016 2nd Int Confer on Electrical, Computer & Telecommunication Engineering (ICECTE)*, 2016, pp. 1-4, doi: 10.1109/ICECTE.2016.7879621
- [9] AM. Sharaf, AAA. El-Gammal, "Multi-objective PSO/GA optimization control strategies for energy efficient PMDC motor drives" *Eur Trans Electr Power*, 2011, 21(8), 2080-2097
- [10] MC. Joshi and S. Samanta, "Modeling and Control of Bidirectional DC-DC Converter Fed PMDC Motor for Electric Vehicles" *2013 Annual IEEE India Conference (INDICON)*, 2013, 10.1109/INDICON.2013.6726091.
- [11] A. Hassoune, M. Khafallah, A. Mesbahi, T. Bouragba, "Power Management Strategies of Electric Vehicle Charging Station Based Grid Tied PV-Battery System" *Int Journal of Renew Energy Research*, 2018, 8(2), 851-60.
- [12] J. Jiang, Y. Bao, LY. Wang, "Topology of a Bidirectional Converter for Energy Interaction between Electric Vehicles and the Grid" *Energies*, 2014, 7, 4859-94.
- [13] AB. Ramaiaha, R. Maurya, SR. Arya, "Bidirectional converter for electric vehicle battery charging with power quality features" *Int Trans on Electr Energy Syst*, 2018, 28, 1-19.
- [14] A. Mendoza-Torres, N. Visairo, C. Nuñez, J. Armenta, E. Rodríguez, I. Cervantes, "Switching rule for a bidirectional DC/DC converter in an electric vehicle", *Control Engg Practice*, 2019, 82, 108-117.
- [15] MC. Joshi, "Modeling and Control of Bidirectional DC DC Converter Fed PMDC Motor" *M.Tech Thesis 2013*, NIT-Rourkella, India.
- [16] CK. Das, SK. Swain, "Closed Loop Speed Control of Chopper Fed DC Motor for Industrial Drive Application", *IEEE Int Conf on Power and Embedded Drive Control (ICPEDC)*, 2017, DOI: 10.1109/ICPEDC.2017.8081137.
- [17] ZM. Tun, TL. Naing, "Double Loop Control of H-Bridge DC Chopper Fed Permanent Magnet DC Motor Drives Using Low Cost Hardware", *International Scholarly and Scientific Research & Innovation*, 2018, 12(11), 857-866.
- [18] AJ. Humaidi, IK. Ibraheem, "Speed Control of Permanent Magnet DC Motor with Friction and Measurement Noise Using Novel Nonlinear Extended State Observer-Based Anti-Disturbance Control", *Energies*, 2019, 12, 1651, 1-22.
- [19] SA. Salman, ZA. Obaid, HS Hameed, "Stability and performance evaluation of the speed control of DC motor using state-feedback controller", *Indonesian Journal of Electrical Engineering and Computer Science*, 2021, 22(3), 1372-1378.

- 
- [20] A. Rinc'on, F. Angulo, F. Hoyos, "Controlling a DC Motor through Lypaunov-like Functions and SAB Technique," *International Journal of Electrical and Computer Engineering*, 2018, 8(4), 2180-2198.
  - [21] OW. Abdulwahhab, "Design of an adaptive state feedback controller for a magnetic levitation system," *International Journal of Electrical and Computer Engineering (IJECE)*, 2020, 10(5), 4782-4788.
  - [22] D. Altun, "Performance comparison of fuzzy logic and PID controller for speed control of DC motor in distribution grid," *International Research Journal of Engineering and Technology (IRJET)*, 2019, 6(2), 649-654
  - [23] H. Velasco-Muñoz, JE. Candelo-Becerra, FE. Hoyos, A. Rincón, "Speed Regulation of a Permanent Magnet DC Motor with Sliding Mode Control Based on Washout Filter", *Energies*, 2022, 14, 728, 1-25.
  - [24] SA. Bhatti, SA. Malik, A. Daraz, "Comparison of P-I and I-P controller by using Ziegler-Nichols tuning method for speed control of DC motor", *IEEE Int Conf on Intelligent Systems Engineering (ICISE)*, 2016, 330-334.